
White Rose Research Online

eprints@whiterose.ac.uk
https://eprints.whiterose.ac.uk
Universities of Leeds, Sheffield and York

Deposited via The University of Sheffield.

White Rose Research Online URL for this paper:
https://eprints.whiterose.ac.uk/id/eprint/824/

Article:
Wang, J.B., Xia, Z.P. and Howe, D. (2005) Three-phase modular permanent magnet brushless machine for torque boosting on a downsized ICE vehicle. IEEE Transactions on Vehicular Technology, 54 (3). pp. 809-816. ISSN: 0018-9545

https://doi.org/10.1109/TVT.2005.847224

Reuse
Items deposited in White Rose Research Online are protected by copyright, with all rights reserved unless indicated otherwise. They may be downloaded and/or printed for private study, or other acts as permitted by national copyright laws. The publisher or other rights holders may allow further reproduction and re-use of the full text version. This is indicated by the licence information on the White Rose Research Online record for the item.

Takedown
If you consider content in White Rose Research Online to be in breach of UK law, please notify us by emailing eprints@whiterose.ac.uk including the URL of the record and the reason for the withdrawal request.



Three-Phase Modular Permanent Magnet Brushless Machine for Torque Boosting on a Downsized ICE Vehicle

Jiabin Wang, *Senior Member, IEEE*, Zhen Ping Xia, and David Howe

***Abstract*—The paper describes a relatively new topology of 3-phase permanent magnet (PM) brushless machine, which offers a number of significant advantages over conventional PM brushless machines for automotive applications, such as electrical torque boosting at low engine speeds for vehicles equipped with downsized internal combustion engine (ICEs). The relative merits of feasible slot/pole number combinations for the proposed 3-phase modular PM brushless ac machine are discussed, and an analytical method for establishing the open-circuit and armature reaction magnetic field distributions when such a machine is equipped with a surface-mounted magnet rotor is presented. The results allow the prediction of the torque, the phase emf, and the self- and mutual winding inductances in closed forms, and provide a basis for comparative studies, design optimization and machine dynamic modeling. However, a more robust machine, in terms of improved containment of the magnets, results when the magnets are buried inside the rotor, which, since it introduces a reluctance torque, also serves to reduce the back-emf, the iron loss and the inverter voltage rating. The performance of a modular PM brushless machine equipped with an interior magnet rotor is demonstrated by measurements on a 22-pole/24-slot prototype torque boosting machine.**

***Index Terms*—Electric torque boosting, engine downsizing, hybrid electric vehicle, permanent magnet (PM) machine.**

I. Introduction

THE need to improve fuel efficiency and reduce the emission of CO_2 and other harmful pollutants from internal combustion engine (ICE) vehicles has led to a significant demand for hybridization of vehicle power-trains [1]–[3]. There are three main power-train configurations for hybrid electric vehicles, *viz.*, series hybrid, parallel hybrid, and series parallel hybrid [4], [5]. In a series hybrid configuration, an ICE drives an electric generator which provides power to the vehicle traction motor and the energy storage buffer, battery for example. In a parallel hybrid electric vehicle, the ICE and electric motor are coupled directly or via a gearbox by clutches. By appropriately controlling the clutch and power electronic converter, it is possible to drive the vehicle only with the electric motor, with the ICE (the electric motor in idle) or with both the electric motor and ICE. The motor can also be driven by the ICE and operates in generation mode to charge the battery. The introduction of a mechanical coupling via a clutch between the generator and electric motor enables the vehicle power-train to change from a parallel configuration to a series configuration, or vice versa, hereby offering more flexibility in terms of optimally apportioning the energy sources under various drive conditions. In all three different configurations, the hybridization factor, i.e., the ratio of the motor power rating to that of ICE tends to be relatively high, which lead to a significant increase in vehicle cost.

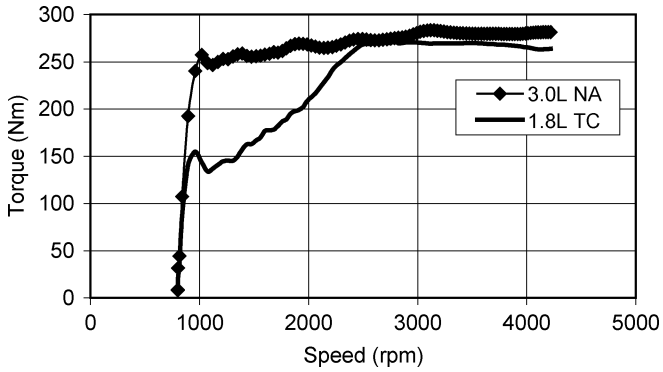

Fig. 1. Typical torque-speed characteristics of 3.0 L naturally aspirated (NA) and 1.8 L turbocharged (TC) ICEs (Courtesy of FEV, Germany).

Recently, a new form of hybridization known as engine-downsizing has been proposed [6]. Small, lightweight supercharged ICEs can reduce fuel consumption by ∼30% compared to standard ICEs with ∼40% higher displacement. However, supercharged ICEs exhibit a relatively poor torque capability at low engine speeds, which results in unacceptable drive-away and acceleration performance, as illustrated in Fig. 1 [6]. However, the low speed torque deficit may be overcome by employing an electrical machine, supplied from an auxiliary energy storage system, such as a supercapacitor, to provide a torque boost for short periods. Fig. 2 shows a schematic of a vehicle power-train equipped with such an electrical torque boost system. At low engine speeds, the supercapacitor unit supplies energy to the electrical machine which provides the required level of torque boosting to improve the drive-away and acceleration capabilities of the vehicle. The supercapacitors may be recharged either by regeneration from the electrical machine, when the engine speed is sufficiently high or vehicle kinetic energy is being recovered during braking, or via the dc/dc converter, using energy which is stored in the battery. The latter may be necessary if the vehicle is not used for protracted periods when the supercapacitor unit may become discharged. The electrical machine could also perform the alternator and

Manuscript received September 28, 2004; revised December 10, 2004 and January 30, 2005. The review of this paper was coordinated by Prof. A. Emadi.

The authors are with the Department of Electronic and Electrical Engineering, University of Sheffield, Sheffield, S1 3JD, U.K. (e-mail: j.b.wang@sheffield.ac.uk).

Digital Object Identifier 10.1109/TVT.2005.847224

0018-9545/$20.00 © 2005 IEEE

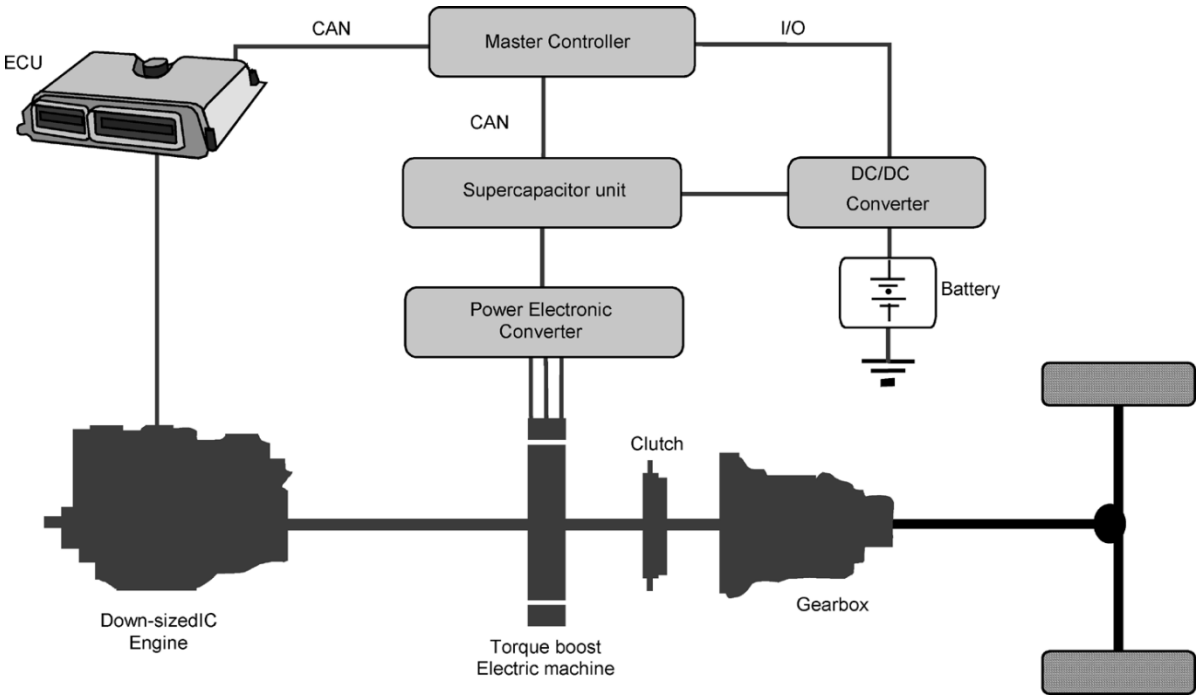

Fig. 2. Downsized ICE vehicle with supercapacitor-based torque booster (Courtesy of EST project partners).

engine starter functions. Since the torque boosting is only required at low engine speeds, and average power rating of the electric power components is significantly lower than that of conventional mild hybrid power-train configurations, this form of power-train configuration becomes particularly attractive to low cost applications.

As will be seen from various hybrid electric vehicle formats, the electric machine, whether it operates as motor or generator, plays a key role in improving fuel economy, energy efficiency and drive performance. The common requirements for electric machines in this application are high-power/torque density, high-energy efficiency, robust to the harsh operating environment, and low production cost. Brushless permanent magnet (PM) machine technology is arguably well suited for meeting these requirements, as has been demonstrated in commercially available hybrid vehicles such as Toyota Prius [7]. The paper describes a relatively new topology of brushless PM machines, which offer a number of significant advantages over conventional brushless PM machines for hybrid electric vehicle applications, such as providing electric traction torque or boosting torque for a downsized ICE at low engine speeds. Although the paper is concerned with the embodiment of an optimal design for electric torque boosting, the proposed topology could be scaled up and down to suit other hybrid vehicle applications.

In the downsized ICE vehicle power-train configuration, Fig. 2, the intermittent duty and space envelope constraints imposed by the need to integrate the torque boost machine with the ICE and flywheel favor the use of a brushless permanent magnet (PM) machine, due to its high efficiency, high peak power capability and compactness [6]. However, a conventional PM brushless dc machine has a coil span of 120° electrical degrees, which results in a low winding factor for the fundamental (*viz.* 0.866) and does not reduce the effect of the 5th and 7th harmonic fields. Consequently, although the machine has the advantage of short end winding, it suffers from low torque capability and can exhibit a relatively large cogging torque and excessive torque ripple, which may exacerbate the noise and vibration characteristics of the vehicle power-train.

Recently, a relatively new topology of PM brushless machine, which is often referred to as "modular" [8], [9], has emerged which offers a number of significant advantages over conventional PM brushless machine, which make it particularly attractive for automotive applications. The stator winding of a modular PM brushless machine differs from that of conventional brushless dc and AC machines in that the coils which belong to each phase are concentrated and wound on consecutive teeth, as shown in Fig. 3(a), so that the phase windings do not overlap. This is not only a distinct manufacturing advantage [10], but is also conducive to a high copper packing factor, and, hence, a high efficiency [11], and to reducing the likelihood of an interphase fault. It also results in a small number of slots for a given number of poles, e.g., 24-slots for a 22-pole machine, as compared to 33-slots for a conventional brushless dc winding, Fig. 3(b) and a minimum of 66-slots for a conventional brushless ac winding, Fig. 3(c). Further the modular winding arrangement gives rise to a high winding factor for the fundamental, while the effect of the 5th and 7th harmonic fields being significantly reduced. Such a modular winding also yields a fractional number of slots per pole, with the smallest common multiple between the slot number and the pole number being relatively large. Consequently, the cogging torque can be extremely small without the use of skew [12]. Hence, the modular PM machines will have higher torque capability and lower torque ripple than conventional brushless dc or ac permanent magnet machines.

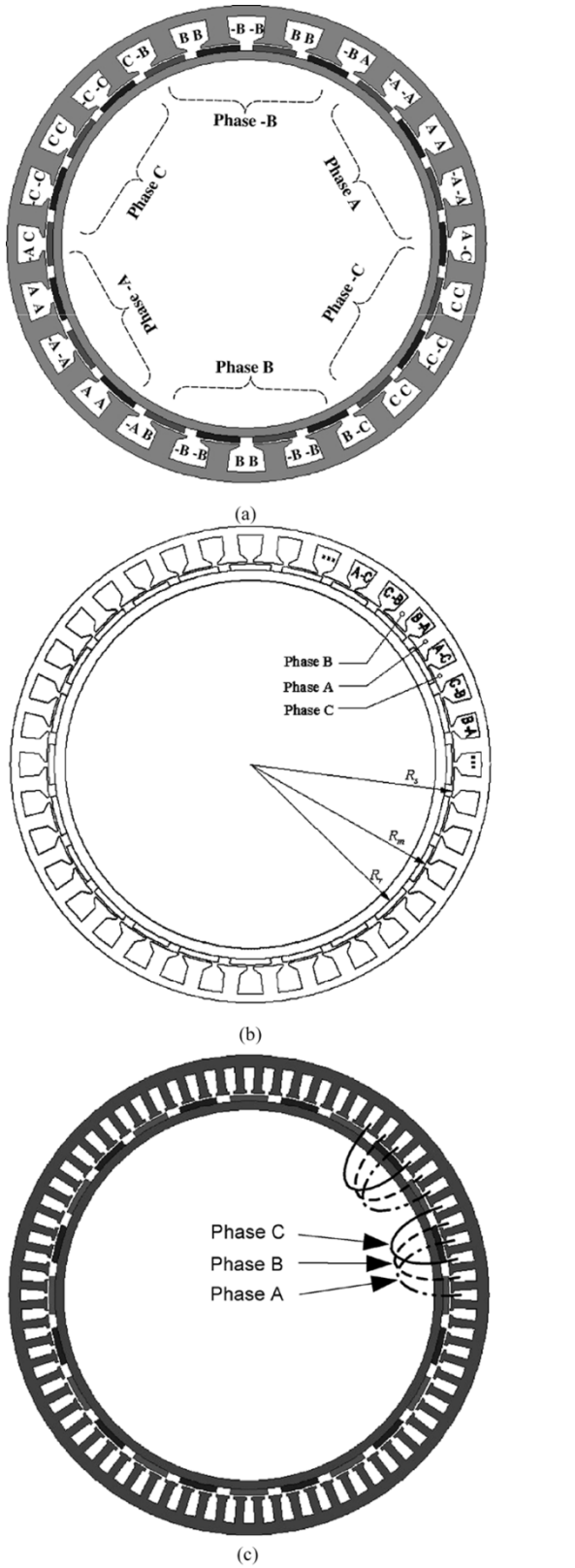

Fig. 3. 3-phase PM brushless machines having three different stator winding configurations. (a) 24-slot/22-pole machine with modular winding. (b) 33-slot/22-pole machine with nonoverlapping winding. (c) 66-slot/22-pole machine with overlapping winding.

This paper discusses the relative merits of feasible slot number and pole number combinations for 3-phase modular PM brushless machines, and presents an analytical method for establishing the open-circuit and armature reaction magnetic field distributions of modular machines equipped with a surface-mounted magnet rotor. The developed analytical framework allows the prediction of the torque, the phase emf, and the self- and mutual winding inductances in closed forms, which, in turn, provides a basis for comparative studies, design optimization and machine dynamic modeling. However, in order to improve the robustness of the machine, the permanent magnets can be buried inside the rotor, which, since it introduces a reluctance torque, also serves to reduce the back-emf, the iron loss and the inverter voltage rating. The performance of such a 3-phase modular brushless PM machine is demonstrated by measurements on a prototype 24-slot/22-pole machine which has been developed for the electrical torque-boost system which is illustrated in Fig. 2. However, 3-phase modular brushless machines would also be eminently suitable for other applications on hybrid and electric vehicles, such as traction drives and generators.

II. Feasible Slot/ Pole Combinations

Many feasible slot and pole combinations exist for three-phase modular PM machines, the slot number N_s being related to the number of pole-pairs p by the following

$$N_s = 2p \pm 1 \text{ or } 2p \pm 2 \tag{1}$$

where N_s must be divisible by 3. Furthermore, for a three-phase winding, the phase shift between phases is given by

$$\begin{aligned}\theta_{ps} &= \beta_s * \frac{N_s}{3} * \frac{180}{\beta_p} \\ &= \frac{2p\beta_p}{Ns} * \left(\frac{N_s}{3} * \frac{180}{\beta_p}\right) = \frac{360p}{3}\end{aligned} \tag{2}$$

which, in electrical degrees, must equal $\pm 360k + 120$, where $k = 0, 1, 2, \ldots$ is a positive integer, β_p is the magnet pole-pitch angle, and $\beta_s = 2p\beta_p/Ns$ is the slot-pitch angle.

Table I lists all possible combinations of N_s and p derived from (1) and (2). It should be noted, from (2), that there is no feasible slot/pole number combination when p is divisible by 3. For all feasible $N_s = 2p \pm 1$ combinations, the number of slots per phase is odd. Therefore, all the coils which form one phase must be connected in series since the emf which is induced in each coil is not exactly in phase. In other words, such slot/pole number combinations prevent the coils from being interconnected to form phase windings with parallel paths. As p increases, the number of coils in series also increases, and, as will be shown, the winding factor decreases, which will adversely affect the machine performance. For all feasible $N_s = 2p \pm 2$ combinations, however, the number of slots per phase is even. Therefore, the coils of each phase can be either all connected in series or connected in series/parallel groups if p is even or series/anti-parallel groups if p is odd.

Thus, $N_s = 2p \pm 2$ slot/pole combinations offer greater flexibility in that the number of parallel paths may be greater than 1. It will also be noted that for a given N_s/p combination multiplication of both p and N_s by a positive integer number results in a new feasible slot/pole combination. For example, for $N_s/p = 9/4$, $N_s/p = 18/8, 27/12, 36/16, \ldots$, etc, are also

TABLE I
FEASIBLE SLOT COMBINATIONS FOR $2p \pm 1$, AND $2p \pm 2$

	Feasible slot number, N_s	
Number of pole-pairs, p	$2p$±1	$2p$±2
1	3	-
2	3	6
4	9	6
5	9	12
7	15	12
8	15	18
10	21	18
11	21	24
13	27	24
14	27	30
16	33	30
17	33	36
19	39	36
20	39	42
22	45	42
23	45	48
…	…	…

TABLE II
FEASIBLE POLE/SLOT COMBINATIONS FOR THREE-PHASE MODULAR PM MACHINES

Number of pole-pairs, p	Number of slots, N_s
1	3
2	3, 6
3	9
4	6, 9, 12
5	9, 12, 15
6	9, 18
7	12, 15, 21
8	12, 15, 18, 24
9	27
10	18, 21, 24, 30
11	21, 24, 33
12	18, 27, 36
13	24, 27, 39
14	24, 27, 30, 42
15	27, 36, 45
16	24, 30, 33, 36, 48
17	33, 36, 51
18	27, 54
19	36, 39, 57
20	30, 36, 39, 42, 45, 48, 60

feasible combinations, some of which are not cited in Table I. In addition, although values of p which are integer multiples of 3 are not included in Table I, new slot/pole combinations for such pole numbers can be derived from integer multiples of the N_s/p combination for $p = 1$. In general, as the number of pole-pairs increases, the number of feasible combinations of N_s and p becomes greater. For instance, when $p = 8$, there are 4 feasible combinations, *viz.* $N_s/p = 12/8$, 15/8, 18/8, and 24/8, while when $p = 16$, 5 feasible combinations exist, *viz.* $N_s/p = 24/16$, 30/16, 33/16, 36/16, and 48/16. It is evident that modular machines with an even number of pole-pairs have more feasible slot/pole number combinations than those having an odd number of pole-pairs. Table II summarizes all feasible combinations for values of p up to 20, where it will be noted that the last value of N_s in each row corresponds to the slot/pole number combination of a conventional PM brushless dc machine.

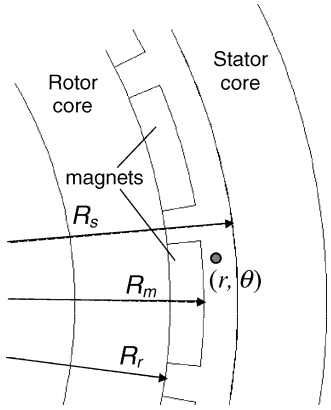

Fig. 4. Analytical model for surface-mounted magnet PM machine.

For a given number of pole-pairs, different slot combinations lead to different winding factors for both the fundamental and high order emf harmonics, and for the armature reaction mmf distribution. Further, the cogging torque due to slotting is approximately related to the inverse of the smallest common multiple of p and Ns [12]. Thus, the choice of a particular slot/pole combination has a profound influence on the performance, demagnetization withstand capability and noise/vibration characteristics of a machine.

III. OPEN-CIRCUIT MAGNETIC FIELD DISTRIBUTION, FLUX-LINKAGE AND EMF

For a surface-mounted magnet machine having the geometry shown in Fig. 3(a), the open-circuit air-gap magnetic field distribution can be derived analytically using the model shown in Fig. 4 [13].

The radial and tangential flux density components, as functions of r and θ, are given by

$$B_r(r,\theta) = \sum_{n=1,3,5,\ldots}^{\infty} K_B(n) f_{Br}(r) \cos(np\theta)$$
$$B_\theta(r,\theta) = \sum_{n=1,3,5\ldots}^{\infty} K_B(n) f_{B\theta}(r) \sin(np\theta) \quad (3)$$

where $K_B(n)$, $f_{Br}(r)$, $f_{B\theta}(r)$ can be derived using the technique reported in [13], and given by

$$K_B(n) = \frac{\mu_0 M_n}{\mu_r} \frac{np}{(np)^2 - 1} \times \left\{ \frac{(np-1)+2\left(\frac{R_r}{R_m}\right)^{np+1} - (np+1)\left(\frac{R_r}{R_m}\right)^{2np}}{\frac{\mu_r+1}{\mu_r}\left[1-\left(\frac{R_r}{R_s}\right)^{2np}\right] - \frac{\mu_r-1}{\mu_r}\left[\left(\frac{R_m}{R_s}\right)^{2np} - \left(\frac{R_r}{R_m}\right)^{2np}\right]} \right\} \quad (4)$$

$$f_{Br}(r) = \left(\frac{r}{R_s}\right)^{np-1} \left(\frac{R_m}{R_s}\right)^{np+1} + \left(\frac{R_m}{r}\right)^{np+1} \quad (5)$$

$$f_{B\theta}(r) = -\left(\frac{r}{R_s}\right)^{np-1} \left(\frac{R_m}{R_s}\right)^{np+1} + \left(\frac{R_m}{r}\right)^{np+1} \quad (6)$$

for $np \neq 1$ and

$$K_B(n) = \frac{\mu_0 M_n}{\mu_r} \times \left\{ \frac{\left(\frac{R_m}{R_s}\right)^2 - \left(\frac{R_r}{R_s}\right)^2 + \left(\frac{R_r}{R_s}\right)^2 \ln\left(\frac{R_m}{R_r}\right)^2}{\frac{\mu_r+1}{\mu_r}\left[1-\left(\frac{R_r}{R_s}\right)^2\right] - \frac{\mu_r-1}{\mu_r}\left[\left(\frac{R_m}{R_s}\right)^2 - \left(\frac{R_r}{R_m}\right)^2\right]} \right\} \quad (7)$$

$$f_{Br}(r) = 1 + \left(\frac{R_s}{r}\right)^2$$

$$f_{B\theta}(r) = -1 + \left(\frac{R_s}{r}\right)^2 \quad (8)$$

for $np = 1$, where θ is the mechanical angular position with reference to the center of a magnet pole, α_p is the ratio of the magnet pole-arc to pole-pitch, and R_s, R_r, and R_m are the stator bore radius and the radii of inner and outer rotor magnets, respectively. For radially magnetised magnets M_n is given by

$$M_n = \frac{2B_r\alpha_p}{\mu_0} \frac{\sin\left(\frac{n\pi\alpha_p}{2}\right)}{\frac{n\pi\alpha_p}{2}}. \quad (9)$$

The open-circuit flux-linkage of a phase coil having T_c turns may be obtained by integrating B_r at the stator bore $r = R_s$ over the slot-pitch angle β_s

$$\Psi_C = T_C \int_{\omega_m t - \frac{\beta_s}{2}}^{\omega_m t + \frac{\beta_s}{2}} B_r(R_s, \theta_r) R_s L_{stk} d\theta = 2R_s L_{stk} T_C \sum_{n=1,3,\ldots}^{\infty} K_{rn} \frac{1}{np} K_{pn} \cos(np\omega_m t) \quad (10)$$

where $K_{rn} = K_B(n) f_{br}(R_s)$, L_{stk} is the stator stack length, and K_{pn} is the pitch factor of the n^{th} harmonic, given by

$$K_{pn} = \sin\left(\frac{np\beta_s}{2}\right). \quad (11)$$

The induced emf in a phase coil is, therefore, given by

$$e_c = -\frac{d\psi_c}{dt} = 2T_c R_s L_{stk} \omega_m \sum_{n=1,3,\ldots}^{\infty} K_{rn} K_{pn} \sin(np\omega_m t). \quad (12)$$

In a modular machine, the emfs in two adjacent coils are displaced by an electrical angle given by

$$\theta_d = \frac{abs(\beta_p - \beta_s)\pi}{\beta_p}. \quad (13)$$

The emf in a phase winding having N_{sp} coils connected in series can, therefore, be obtained as

$$e_p = 2T_c N_{sp} R_s L_{stk} \omega_m \sum_{n=1,3,\ldots}^{\infty} K_{rn} K_{pn} K_{dn} \times \sin\left(np\omega_m t + n(N_{sp}-1)\frac{\theta_d}{2}\right) \quad (14)$$

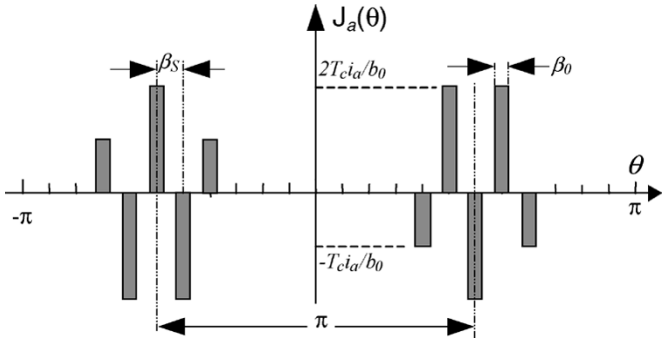

Fig. 5. Mmf distribution of a phase winding.

where K_{dn} is the distribution factor of the n^{th} harmonic, given by

$$K_{dn} = \frac{\left\{\sin\left(\frac{nN_{sp}\theta_d}{2}\right)\right\}}{\left\{N_{sp}\sin\left(\frac{n\theta_d}{2}\right)\right\}}. \quad (15)$$

It should be noted that the winding factors $(K_{dn}K_{pn})$ for the 1st (fundamental), 5th and 7th harmonics of the 24-slot/22-pole modular machine are 0.95, 0.16 and 0.1, respectively, as compared with 0.866, -0.866 and 0.866 of the 33-slot/22-pole bruchless dc machine. Consequently, for the same size, and the same electrical and magnetic loadings, the modular machine has $\sim$9% higher torque capability and a much lower torque ripple than the brushless dc machine.

IV. Armature Reaction Field and Inductance

The armature reaction field in a surface-mounted magnet modular PM machine can also be derived analytically, based on the assumption that the stator and rotor cores are infinitely permeable [14]. By way of example, Fig. 5 shows the magneto-motive force (mmf) distribution of the phase A winding in the 24-slot/22-pole modular machine shown in Fig. 3(a), which may be represented by a Fourier series of the following form

$$J_a(\theta) = \sum_{n=1}^{\infty} i_a J_n \sin(n\theta) \quad (16)$$

where b_0 is the width of the slot openings, β_0 is the corresponding slot opening angle, and

$$J_n = 4\left(\frac{4T_c}{\pi R_s}\right) K_{dcn} K_{pcn} \quad (17)$$

$$K_{dcn} = \frac{\sin\left(\frac{n\beta_0}{2}\right)}{\left(\frac{n\beta_0}{2}\right)} \quad (18)$$

[see (19) at the bottom of the next page]. Fig. 6 shows the air-gap mmf harmonic distribution of the three-phase modular winding normalized to the coil Ampere turns, $(T_c I_m)$. As will be seen, the mmf contains forward rotating harmonics for $n = 5, 11, 19, \ldots$, backward rotating harmonics for $n =$ for $n = 1, 7, 13, \ldots$, and zero even and triplen harmonics. It is also evident that the 11th, 13th, 35th, 37th, . . ., harmonics are dominant.

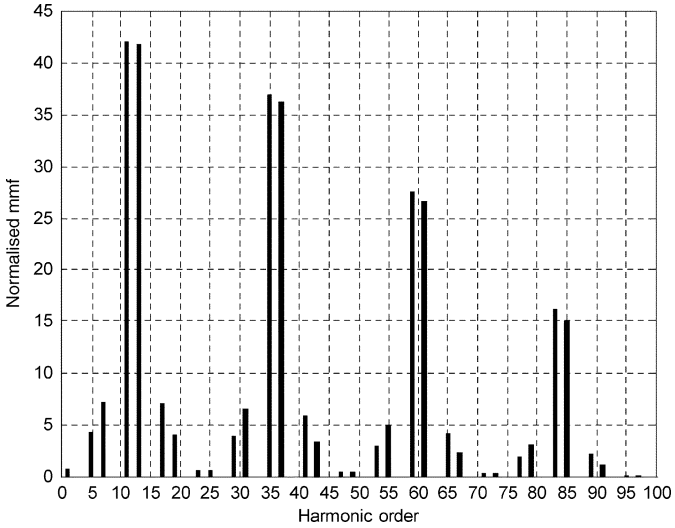

Fig. 6. Normalized mmf harmonic distribution.

Thus, for this particular 24-slot three-phase modular winding arrangement, feasible numbers of pole-pairs for the machine are 11, 13, 35, 37, ..., etc. As the number of pole-pairs increases, however, interpole leakage becomes greater, which may compromise the torque capability. It should also be noted that the wavelength of the lowest field harmonic is $2\pi R_s$, although its magnitude is relatively small. For the 22-pole machine, however, only the 11th mmf harmonic interacts with the magnetic field of the permanent magnets to produce continuous torque. The other harmonics, in particular the 13th, 35th, 37th, ..., etc., which have relatively large magnitudes, may cause undesirable effects, such as localized core saturation, and eddy current loss in the magnets, which is the main disadvantage of modular machines. However, the eddy current loss in the rotor magnets of a modular machine is not significantly higher than that in a conventional brushless dc machine, and can be effectively reduced by segmentation of the rotor magnets [15].

The resulting armature reaction flux density components in the permanent magnets and the air-gap are given by

$$B_{ar} = \mu_o i_a \sum_{n=1}^{\infty} J_n F_{ar}(r)\cos(n\theta)$$
$$B_{a\theta} = -\mu_o i_a \sum_{n=1}^{\infty} J_n F_{a\theta}(r)\sin(n\theta) \tag{20}$$

where

$$F_{ar}(r) = \frac{1+\left(\frac{R_r}{r}\right)^{2n}}{1-\left(\frac{R_r}{R_s}\right)^{2n}}\left(\frac{r}{R_s}\right)^{n-1} \tag{21-a}$$

$$F_{a\theta}(r) = \frac{1-\left(\frac{R_r}{r}\right)^{2n}}{1-\left(\frac{R_r}{R_s}\right)^{2n}}\left(\frac{r}{R_s}\right)^{n-1}. \tag{21-b}$$

Fig. 7. Prototype machine.

Equation (20) forms the basis for evaluating whether any partial irreversible demagnetization of the magnets occurs under a specific operating condition.

The air-gap self-inductance L_{as} and mutual inductance M_{aij} can be obtained by evaluating the flux-linkage due to the armature reaction field, and are given by

$$L_{as} = \frac{\mu_o 4 L_{stk}(8T_c)^2}{\pi} \times \sum_{n=1}^{\infty} \frac{F_{ar}(R_s)(K_{dcn}K_{pcn})^2}{n} \tag{22}$$

$$M_{aij} = \frac{\mu_o 4 L_{stk}(8T_c)^2}{\pi} \times \sum_{n=1}^{\infty} \frac{F_{ar}(R_s)(K_{dcn}K_{pcn})^2}{n}\cos(n\beta_{ij}) \tag{23}$$

where β_{ij} is the mechanical angular difference between phases i and j. For a slotted armature, however, slot leakage will also contribute to the self and mutual inductances. The total self and mutual inductances of the machine are, therefore, given by

$$L_s = L_{as} + L_{sk}; \quad M_{ij} = M_{aij} + M_{sk} \tag{24}$$

where the slot leakage components L_{sk} and M_{sk} can be evaluated using formulas given in [16].

V. Prototype and Experimental Results

For many automotive applications, such as electrical torque boosting, the maximum rotor speed is typically around 6000 rpm. Thus, retention of the rotor magnets is a major consideration. However, although the magnets might be contained within a metallic, nonmagnetic sleeve or by fiber reinforced banding, for convenience, the magnets in the prototype 24-slot/22-pole modular torque boost machine were contained in slots within the laminated rotor, a prototype of which is shown in Fig. 7 and whose performance specification is given in Table III. Fig. 8

$$K_{\rm pcn} = \frac{[-0.5\sin(n4\beta_s) + \sin(n5\beta_s) - \sin(n6\beta_s) + \sin(n7\beta_s) - 0.5\sin(n8\beta_s)]}{4}. \tag{19}$$

TABLE III
DESIGN SPECIFICATIONS FOR PROTOTYPE MODULAR PM MACHINE

Rated output power (kW)	18.5
Rated speed (rpm)	1700
Rated torque (Nm)	105
Rate phase current (rms A)	345
Peak torque (Nm)	140
DC link voltage (V)	60

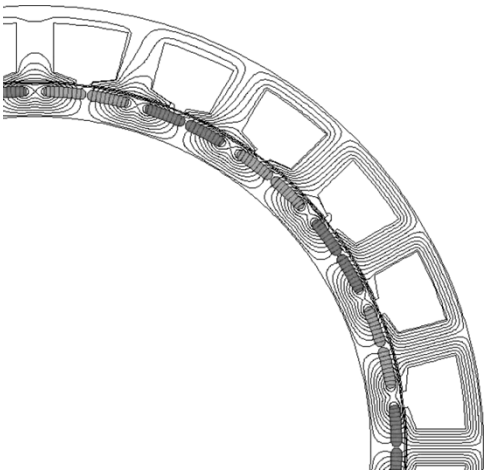

Fig. 8. Open-circuit magnetic field distribution in 24-slot/22-pole modular brushless PM machine.

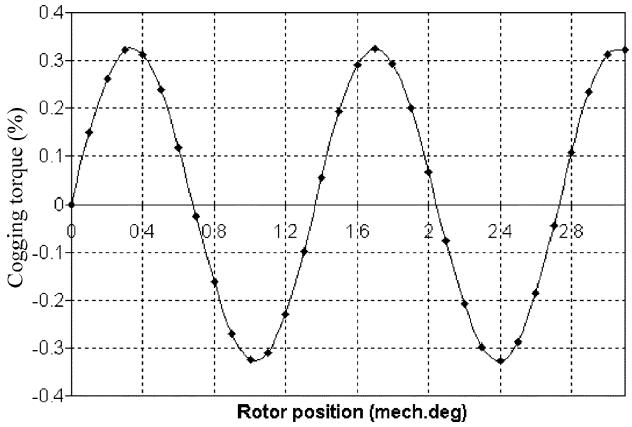

Fig. 9. Cogging torque waveform of 24-slot/22-pole modular machine.

shows the finite element predicted open-circuit magnetic field distribution, while Fig. 9 shows the cogging torque waveform of the prototype machine. As can be seen, the cogging torque which results with the modular machine topology is extremely low, being less than 0.3% of the rated torque. Fig. 10(a) and (b) compares the measured and predicted phase self-inductance and back-emf as functions of the rotor position. As will be seen, the measurements and predictions are in good agreement, and, it should be noted that, while the inductance varies with the rotor angular position, the degree of saliency which can be achieved is limited by the available rotor space envelope, which is constrained by the ICE-clutch arrangement. Nevertheless, an interior-magnet rotor is also beneficial in terms of reducing the idling loss and inverter voltage rating. Fig. 11 and Table IV

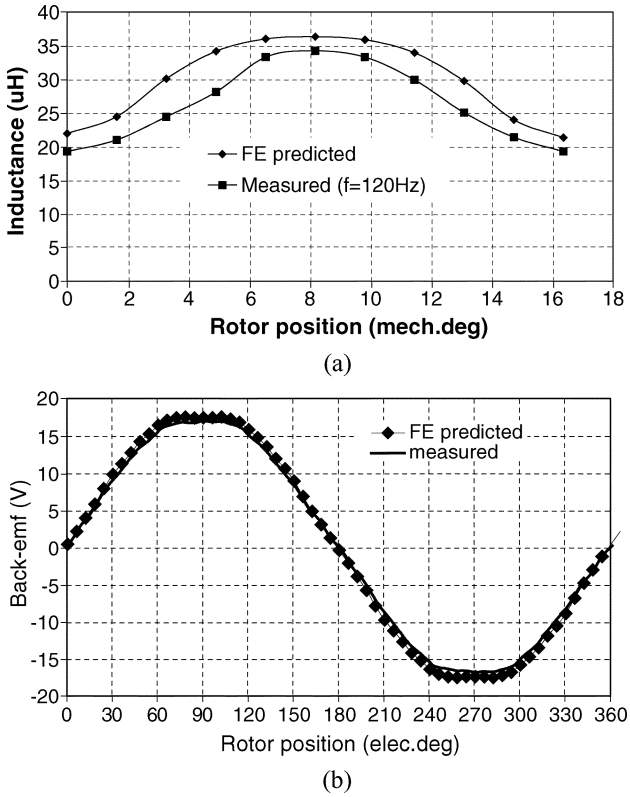

Fig. 10. Comparison of measured and predicted phase inductance and back-emf. (a) Inductance. (b) Back-emf at 1000 rpm.

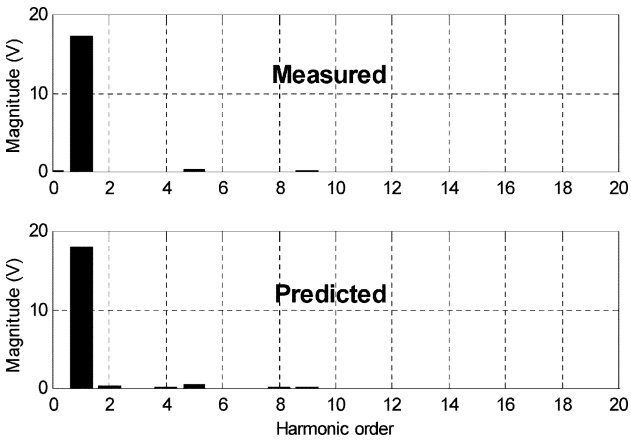

Fig. 11. Comparison of measured and predicted back-emf harmonic distributions.

TABLE IV
COMPARISON OF BACK-EMF HARMONIC COMPONENTS

Harmonic order	1	3	5	7
Predicted	18.02	0.05	0.50	0.04
Measured	17.26	0.04	0.35	0.06

compare measured and predicted harmonic components in the back-emf waveform, from which it is evident that the modular machine has very low fifth and seventh emf harmonics. Thus, the machine has a very low torque ripple when the stator is supplied with sinusoidally time-varying phase currents.

VI. Conclusion

The utility and design considerations for 3-phase modular PM brushless ac machines have been described, with particular reference to a torque-boost machine for a downsized ICE vehicle. Feasible slot number and pole number combinations for such machines have been derived, and their relative merits have been discussed. It has been shown that various feasible combinations exist for a given number of pole-pairs, and that the choice of a particular slot number/pole number combination has a significant influence on the machine performance, such as the magnitude of the cogging torque and the demagnetization withstand capability. Analytical formulae for predicting the open-circuit and armature reaction magnetic field distributions of a modular machine equipped with a surface-mounted magnet rotor have been established. These allow the prediction of the torque, the phase emf, and the self- and mutual winding inductances in closed forms, and provide a basis for comparative studies, design optimization and machine dynamic modeling. The performance of a 22-pole/24-slot 3-phase modular PM brushless machine, equipped with an interior-magnet rotor so as to improve robustness, for an electrical torque-boost system has been verified by measurements. However, given that modular machines are simpler to manufacture and offer improved performance and reliability compared with conventional 3-phase PM brushless machines, they should be attractive for other automotive applications which require energy efficient and power dense electrical machines.

References

[1] H. Kahlen and G. Maggetto, "Eectric and hybrid vehicles," in *Proc. EPE97*, Trondheim, 1997, pp. 1030–1054.

[2] C. C. Chan, "The state of the art of electric and hybrid vehicles," *Proc. IEEE*, vol. 90, pp. 247–275, 2002.

[3] J. M. Miller, A. Emadi, A. V. Rajarathnam, and M. Ehsani, "Current status and future trends in more electric car power systems," in *Proc. 1999 IEEE Veh. Technol. Conf.*, Houston, TX, May 1999, pp. 1380–1384.

[4] S. Barsali, C. Miulli, and A. Possenti, "A control strategy to minimize fuel consumption of series hybrid electric vehicles," *IEEE Trans. Energy Convers.*, vol. 19, no. 1, pp. 187–195, 2004.

[5] S. M. Lukic and A. Emadi, "Effects of drivetrain hybridization on fuel economy and dynamic performance of parallel hybrid electric vehicles," *IEEE Trans. Veh. Technol.*, vol. 53, no. 2, pp. 385–389, 2004.

[6] J. Wang, Z. P. Xia, B. Taylor, and D. Howe, "Supercapacitor-based torque booster for down-sized ICE vehicle," in *Proc. PEMD2004*, Edinburgh, U.K., Mar. 31–Apr. 2 2004.

[7] Toyota PLC, *Toyota Prius Driver's Handbook*, 2004.

[8] K. Atallah and D. Howe, "Modular permanent magnet brushless machines for aerospace and automotive applications," in *20th Int. Workshop on Rare-Earth Magnets and Their Applications*, Sendai, Japan, 2000, pp. 1039–1048.

[9] K. Atallah, J. Wang, and D. Howe, "Torque ripple minimization in modular permanent magnet brushless machines," *IEEE Trans. Ind. Appl.*, vol. 36, no. 6, pp. 1689–1695, 2003.

[10] T. Oikawa, T. Tajima, K. Matsumoto, H. Akita, H. Kawaguchi, and H. Kometani, "Development of high efficiency brushless DC motor with new manufacturing method of stator for compressors," in *16th Int. Compressor Eng. Conf.*, Purdue, 2002. CD12-4.

[11] A. G. Jack, B. C. Mecrow, P. G. Dickinson, and D. Stephenson, "Permanent-magnet machines with powdered iron cores and prepressed windings," *IEEE Trans. Ind. Appl.*, vol. 36, no. 4, pp. 1077–1084, 2003.

[12] Z. Q. Zhu and D. Howe, "Influence of design parameters on cogging torque in permanent magnet machines," *IEEE Trans. Energy Convers.*, vol. 15, pp. 407–412, 2000.

[13] Z. Q. Zhu, D. Howe, E. Bolte, and B. Ackermann, "Instantaneous magnetic field distribution in brushless permanent magnet dc motors—part I: open-circuit field," *IEEE Trans. Magnetics*, vol. 29, no. 1, pp. 124–136, 1993.

[14] Z. Q. Zhu and D. Howe, "Instantaneous magnetic field distribution in brushless permanent magnet dc motors—part II: armature reaction field," *IEEE Trans. Magnetics*, vol. 29, no. 1, pp. 136–142, 1993.

[15] H. Toda, Z. P. Xia, J. Wang, K. Atallah, and D. Howe, "Rotor eddy current loss in permanent magnet brushless machines," *IEEE Trans. Magnetics*, vol. 40, no. 4, pp. 2104–2106, 2004.

[16] J. R. Hendershot Jr. and T. J. E. Miller, "Design of brushless permanent-magnet motors," in *Electrical Design*. New York: Magna Physics, 1994, ch. ch. 5, pp. 5-55–5-61,.

Jiabin Wang (SM'03) was born in Jiangsu Province, China, in 1958. He received the B.Eng. and M.Eng. degrees in electrical and electronic engineering from Jiangsu University of Science and Technology, Zhengjiang, China, in 1982 and 1986, respectively, and the Ph.D. degree in electrical and electronic engineering from the University of East London, London, U.K., in 1996.

Currently, he is a Senior Lecturer with the University of Sheffield, Sheffield, U.K. From 1986 to 1991, he was with the Department of Electrical Engineering, Jiangsu University of Science and Technology, where he was appointed a Lecturer in 1987 and an Associated Professor in 1990. He was a Postdoctoral Research Associate with the University of Sheffield from 1996 to 1997, and a Senior Lecturer at the University of East London from 1998 to 2001. His research interests range from motion control to electromagnetic devices and their associated drives.

Zhen Ping Xia received the B.Eng. and M.Sc. degrees from Zhejiang University, Hangzhou, China, in 1982 and 1985, respectively, and the Ph.D. degree from the University of Sheffield, Sheffield, U.K., in 2002, all in electrical engineering.

Since graduation, she has been with Zhejiang University and the Institute of Metrology, China, the University of Sheffield, and IMRA Europe S.A.S. U.K. Research Center. Currently, she is a Research Associate with the University of Sheffield, working on the design and analysis of permanent magnet brushless machines.

David Howe received the B.Tech. and M.Sc. degrees in electrical power engineering from the University of Bradford, Bradford, U.K., in 1966 and 1967, respectively, and the Ph.D. degree in electrical power engineering from the University of Southampton, Southampton, U.K.

Currently, he is a Professor of Electrical Engineering at the University of Sheffield, Sheffield, U.K., where he heads the Electrical Machines and Drives Research Group. He has held academic posts at Brunel University, London, U.K., and Southampton University, and spent a period in industry with NEI Parsons Ltd., Newcastle-Upon-Tyne, U.K., working on electromagnetic problems related to turbogenerators. His research activities span all facets of controlled electrical drive systems with particular emphasis on permanent-magnet-excited machines.

Dr. Howe is a Fellow of the Institution of Electrical Engineers, U.K, and Fellow of the Royal Academy of Engineering, U.K.